Journal of Physics & Astronomy

Research | Vol 4 Iss 2

Broad Iron Kα Emissions from NGC 3516: Revelation of a Non-Disk Thin-Torus around a Kerr Black Hole with a Detailed Formulation on the Emission Mechanism

Ma JZG*

California Institute of Integral Studies, San Francisco, CA, USA

***Corresponding author:** Ma JZG, California Institute of Integral Studies, San Francisco, CA, USA, Tel: +86-1-386-226-7361; E-mail: ZMa@mymail.ciis.edu

Received: August 03, 2016; **Accepted:** September 16, 2016; **Published:** October 22, 2016

Abstract

ASCA observations present broad iron (Fe) Kα emission lines in Seyfert(-like) AGNs. The line is explained to originate from a thin disk surrounding the central black hole (BH) which is either rotating or non-rotating. Based on previous theoretical and observational studies, we propose a non-disk thin-torus to exist in the inner region of the disk around a Kerr (rotating) BH. We develop the commonly-used thin-disk model to the thin torus model in this special region under the Kerr metric and calculate the profiles of the Fe K α lines. By extending previous work, we formulate in details the emission mechanism in this paper. The spectra of a sample galaxy, NGC 3516, is then revisited. New results are as follows: (1) the central BH is not static but rotating, with a dimensionless specific angular momentum, a>0.4, the best-fit of which is 0.9; (2) the radial position of the thin torus is within (20-40) r_g, where r_g is the gravitational radius of the BH; (3) the inclination angle θ_0 of the observer is smaller than 50°; and, (4) the extension of torus to both sides of the equatorial plane can reach 67.3°. Specifically, simulations expose that the so-called "absorption" feature of the line spectrum around 6.0 keV may not be realistic; and, the humps and troughs of the broad line spectra are contributed by the four types of particles around the central BH.

Keywords: ***Black hole; Fe Kα lines; AGNs; Seyfert; Kerr metric; Photons; NGC***

Introduction

Broad iron (Fe) Kα lines were detected in many Seyfert(-like) galaxies [1-3]. A four-day ASCA exposure of one of them, MCG−6-30-15, yielded a well-resolved, extremely broad profile which was argued to be consistent with an accretion disk, extending down to (6-20) r_g outside either a Schwarzschild black hole (BH) [4] or a Kerr one [5], where $r_g=GM/c^2$ is the gravitational radius of the BH with mass M, while G and c are the gravitational constant and the speed of light, respectively. Similarly, a continuous, five-day ASCA observation of NGC 3516 [6] exhibited that the spectrum fits also either a Schwarzschild BH [7] or a Kerr one [8]. Because any BHs are unable to sit at both static and rotating states at the same time, we are inspired to investigate the physical properties, especially the rotation, of the central BH hosted in Seyfert(-like) galaxies.

Citation: Ma JZG. Broad Iron K α Emissions from Seyfert AGNs: Revelation of a Non-Disk Torus around a Kerr Black Hole. J Phys Astron. 2016;4(2):102.

© 2016 Trade Science Inc.

In fact, a lot of studies had exposed that BHs are very likely to be rotating and the Kerr metric should be taken into account in data-fit modelling [8,9]. More important, in the curved space-time, bound geodesics of particles in the inner region of the disk surrounding the central BH, which extends outside to tens of r_g from the hole's horizon, trace out helix-like spherical orbits, rather than disk-like orbits, between the minimum and maximum latitudes about the equatorial plane of the central hole [10]. Fortunately, this prediction was verified by observations. For example, it was addressed that the detection of a comparable width of the Fe line spectrum to the optical ones implies a hot torus in the inner part of the accretion disk [11]. As a result, Page and Thorne's [12] generalized thin-disk model may not still be valid in the inner region of the disk [13].

This article introduces a non-disk thin-torus model to formulate the spectra contributed by the spherical luminous particles in the Kerr metric and apply it to the diagnoses of the observed Fe Kα lines of NGC 3516. The work is a synthesis and an extension of previous studies [14-24]. Specifically, the data-fit modelling results reported in the prior 2002 Letter [23] claimed that NGC 3516 has a central BH of spin a ~0.95, along with the radial position of an emitting torus r~14 and the observer's inclination angle θ_0 ~30°. As an extension, we formulate in details the mechanism of the Fe line emissions in this paper, followed by a revisit to the spectra of NGC 3516. The plan of the paper is as follows: We first describe two coordinate systems and non-disk motions of both particles and photons; then, we present the thin-torus model and numerical calculations within a wide range of three parameters (BH spin a, radial position of the torus r, and observer's inclination angle θ_0); moreover, we predict the rotating state of the central hole in NGC 3516, as well as other relevant parameters by the data-fit simulations; at last, a summary of this work is given in the last Section.

Non-Disk Thin-Torus Formulation of Particles and Photons in Kerr Metric

Coordinates

There are a couple of metrics to be considered, as shown in FIG. 1. One employs the spherical coordinates in the 3D Minkowski space, and the other does the Boyer-Lindquist ones in the 4D Kerr spacetime. With respect to an arbitrary point (t, $r=r_0$, $\theta=\theta_0$, $\varphi=\varphi_0=0$) in the Kerr metric, a distant observer is at rest in the image plane of a celestial sphere at infinity with a polar angle α and an azimuthal angle β in the Minkowski space. The image plane contains the origin of coordinates and perpendicular to the observer's line of sight. In the figure, shadowed region represents the torus at r with a thickness of δr between the minimum and maximum latitudes (two black bands) about the equatorial plane of the central BH in the x−y plane. Part of the Fe Kα photons emitted by the torus particles enter the solid angle element $d\Omega$ and are observed by the observer. Choose natural units $G=c=1$, and a geometrized radial coordinate r in the unit of r_g. Thus, $r_g=M=1$ and r is dimension-free. In addition, consider Greek indices γ running from 1~4. The Boyer-Lindquist metric turns out to take the following form [14]:

$$ds^2 = -(1-2r/\Sigma)dt^2 - \left[4ar(1-\mu)/\Sigma\right]dtd\varphi + (\Sigma/\Delta)dr^2 + \Sigma d\theta^2 + \left[\Lambda(1-\mu)/\Sigma\right]d\varphi^2 \quad (1)$$

where r, θ, φ, and t are the usual Boyer-Lindquist coordinates; $\Sigma=r^2+\mu a^2$, $\mu=\cos^2\theta$, $\Delta=r^2-2r+a^2$, $\Lambda=(r^2+a^2)^2-\Delta(1-\mu)a^2$, in which $a=J/M^2$ is the specific reduced magnitude of the BH angular momentum J.

Torus orbits of a test particle

General trajectories of a test particle are described by the three constants of motion [15]:

$$\left.\begin{aligned} m\varepsilon &= -k_t \\ mML_z &= k_\varphi \\ (mM)^2 Q &= k_\theta^2 + \mu\left[(aM)^2\left(m^2 - k_t^2\right) + k_\varphi^2/(1-\mu)\right] \end{aligned}\right\} \tag{2}$$

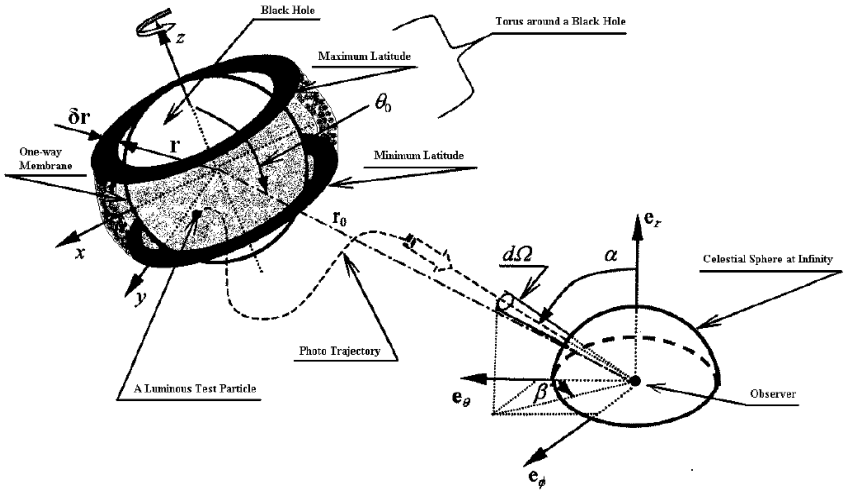

FIG. 1. **Two coordinates for a luminous thin torus (shadowed region) at *r* with a thickness of *δr* in the 4D Kerr metric and a distant observer with respect to the torus in the image plane of a celestial sphere at infinity in the 3D Minkowski space (not drawn to scale), respectively. Bound geodesics of particles trace out helix-like spherical torus orbits between the minimum and maximum latitudes about the equatorial *x*–*y* plane of the central BH. The torus emits broad Fe K*α* photons which can be measured by the observer at the centre of the spherical coordinates which is at {*t*, *r*=*r*₀, *θ*=*θ*₀, *φ*=*φ*₀=0} in the Kerr metric.**

Here m is the rest mass of the particle; ε, L_Z, and Q are the energy reduced by m, angular momentum parallel to the symmetry axis reduced by mM, and Carter's θ-constant reduced by $(mM)^2$, respectively; k_t, k_θ, and k_φ are the three covariant Boyer-Lindquist components of the particle's 4-momentum k^γ at some instant. From Eq. (2) for the k_γ's and thence the k^γ's, the four geodesic equations represented by the 4-velocities u^γ are given by

$$\left.\begin{aligned} \left(\frac{\Sigma}{\varepsilon}\right)u^t &= -a\left[a(1-\mu)-p\right] + \frac{r^2+a^2}{\Delta}\left(r^2+a^2-ap\right) \\ \left[\left(\frac{\Sigma}{\varepsilon}\right)u^r\right]^2 &= R(r) = -\left(\frac{1}{\varepsilon^2}-1\right)r^4 + \frac{2}{\varepsilon^2}r^3 - \left[a^2\left(\frac{1}{\varepsilon^2}-1\right)+\left(p^2+q\right)\right]r^2 + 2\left[(a-p)^2+q\right]r - a^2q \\ \left[\left(\frac{\Sigma}{\varepsilon}\right)u^\theta\right]^2 &= \Theta(\mu) = 4\mu\left\{\left(\frac{1}{\varepsilon^2}-1\right)a^2\mu^2 - \left[a^2\left(\frac{1}{\varepsilon^2}-1\right)+\left(p^2+q\right)\right]\mu + q\right\} \\ \left(\frac{\Sigma}{\varepsilon}\right)u^\varphi &= -\left(a - \frac{p}{1-\mu}\right) + \frac{a}{\Delta}\left(r^2+a^2-ap\right) \end{aligned}\right\} \tag{3}$$

where $p=L_z/\varepsilon$ and $q=Q/\varepsilon^2$. Note that q=0 is the case that the particle is restricted only within the equatorial plane [10,16], which has been widely studied with the thin-disk model since Page and Thorne [12]'s work. The requirement of the third equality in Eq. (3) restricts that $\Theta(\mu) \geq 0$. Thus $0 \leq \mu \leq \mu_-$ (c.f. Eq. (276) in Chandrasekhar's work [25]):

$$90^0 - \cos^{-1}\left(\frac{1}{\sqrt{\mu_-}}\right) \leq \theta \leq 90^0 + \cos^{-1}\left(\frac{1}{\sqrt{\mu_-}}\right) \tag{4}$$

where

$$\mu_{-}=\frac{\left[a^2\left(\frac{1}{\varepsilon^2}-1\right)+\left(p^2+q\right)\right]-\sqrt{\left[a^2\left(\frac{1}{\varepsilon^2}-1\right)+\left(p^2+q\right)\right]^2-4a^2\left(\frac{1}{\varepsilon^2}-1\right)q}}{2a^2\left(\frac{1}{\varepsilon^2}-1\right)}$$

Eq. (4) says that the particles are bounded in a region which is symmetrical about the equatorial plane with the maximal polar angle $\cos^{-1}\left(\mu_{-}^{-1/2}\right)$. A torus particle which is stable in the spherical orbits must satisfy following conditions [10,16]:

$R(r)=\frac{dR}{dr}=\frac{d^2R}{dr^2}=0$. These conditions provide both minimal and maximal expressions of p, then q and ε as follows [22]:

$$p_{\pm}=\frac{-B_2\pm\sqrt{B_2^2-4B_1B_3}}{2B_1}$$

$$q=-\frac{r}{\Delta^2}\left\{\left[r\left(r-2\right)^2-a^2\right]p^2+2a\left[r\left(3r-4\right)+a^2\right]p-\left[\left(r^2+a^2\right)^2-4a^2r\right]\right\} \quad (5)$$

where

$$B_1 = A_2/A_1 - A_5$$
$$B_2 = A_3/A_1 - A_6$$
$$B_3 = -A_4/A_1 + A_7$$
$$A_1 = 5r^4 - 16r^3 + 6(a^2 + 2)\, r^2 - 8a^2r + a^4$$
$$A_2 = \Delta^2(5r^3 - 16r^2 + 12r - 2a^2)$$
$$A_3 = 4a\Delta^2(6r^2 - 6r + a^2)$$
$$A_4 = 2\Delta^2(3r^4 + 4a^2r^2 - 6a^2r + a^4)$$
$$A_5 = r\,(r - 2)^2 - a^2$$
$$A_6 = 2a\,[r(3r - 4) + a^2]$$
$$A_7 = (r^2 + a^2)^2 - 4a^2r$$

Eq. (5) shows that the constants of motion have both lower and upper limits with every set of r and a. Both of the limits correspond to the minimum and maximum latitudes as described in [10]. That is to say, a particle is not merely restricted to either an equatorial plane with q=0 or a tilted one with q to be a specific constant other than q=0; by contrast, it is bounded to a permitted range of q, which corresponds to a region where the torus extends to both sides of the equatorial plane.

Assumptions about particles and photons

According to statistic physics, particles should obey Boltzmann distributions. That is, the number density of particles in an energy interval $\delta\varepsilon$ depends on the energy ε. For simplicity, this paper does not consider the energy distribution. All particles are assumed to have equal probability to take up every set of values of the three constants of motion given by Eq. (5), and there are sufficient particles to take all sets of these values.

The fluorescent photons emitted by the particles detected by the observer in the Minkowski space follow the null geodesics in the Kerr metric (FIG. 1). Their paths are completely described by the initial conditions and two constants of motion, which are expressed by α and β, respectively, of the observer [16,18]. Because photons obey Eq. (3) with m=0 [19,25], the three covariant components, s_t, s_θ, and s_φ, of the 4-momentum are expressed as follows [17,18]:

$$
\begin{aligned}
s_t &= -h\nu \\
s_\theta^2 &= -\frac{(Mh\nu)^2\left[\Sigma\Lambda + 4ar\Sigma x - (\Sigma - 2r)x^2/(1-\mu)\right]}{\Lambda(1-2r/\Sigma) + 4(ar)^2(1-\mu)/\Sigma} \\
s_\varphi &= Mh\nu x
\end{aligned}
\tag{6}
$$

where $x=\rho$ cos β sin θ_0; $\rho=r$ sin α is photon's impact parameter, ν is the detected frequency, and θ_0 is the observer's inclination angle.

Thin-Torus Model and Fe Kα -Line Emissions

Extension of thin-disk model

Early studies used the relativistic generalization of Liouville's theorem to calculate the spectral flux [26-28]. After Thorne's [29] famous contribution to the time-averaged structure of a thin, equatorial disk of the material accreting onto a central BH, Cunningham [9] employed the theorem to give a prediction about the X-ray continuum from the disk.

It was not until Laor [8] that the atomic X-ray line profiles were predicted by using the same thin-disk model. The approach was adopted by most subsequent studies [5,20]. The kernel of the model is featured by the following treatments: (1) the solid angle is a function of both the emission radius r and the frequency shift g; (2) the line radiation is emitted from the innermost radius r_{in} to the outermost one r_{out} of the thin disk; and, (3) the total measured flux is the integration of all the photon emissions over r between the two radii of the disk, while a single value of θ=90° was fixed in advance to denote the thin-disk condition.

Unfortunately, different from the continuum, the Fe Kα-line emission is the fluorescence which originates from the very inner part of an accretion disc [4,30], where particles are bounded in spherical orbits, including those within the disk [10,16,23,24]. The thin-disk model has to be re-considered in dealing with the line emissions. FIG. 1 and equations in the last Section refer to a non-disk formulation, where a luminous thin-torus is connected with complicated parameters in both sets of coordinates, such as, the BH spin, particles' constants of motion, photons' impact parameters, the thickness and the radial position of the torus, and the polar angle of the torus. The complexity of the problem requires that we approach the complete modelling through a series of incremental steps so as to be able to gain increasingly the important insights into dealing with more complicated situations in future studies. We thus tackle a basic situation in this paper by taking:

- a thin-torus model [28]: the torus is not thick geometrically, i.e., its thickness δr «r at radius r, indicating that particles are assumed as a thin-shelled ensemble at r;
- a monochromatic model [5,8]: the emission is isotropic; the emitted fluorescent Fe Kα-line spectrum from particles is described by a δ -function in frequency; and, every photon is emitted at an energy of 6.35 keV;
- an identical model [17]: torus particles which emit photons are identical to produce the photons which reach the observer.

From Eq. (5), we see that for a given value of a, a torus contains a collection of sets of the three constants of motion, p, q, and ε^2, at radius r. considering the monotonous relationship between p and q (or ε^2), the number of the sets can be simply represented by the number of q. Therefore, different from the disk model where the continuum is an integration over r, the line flux here is a superimposition of all the possible individual emissions with every q at a definite position of r.

Line-emissivity law

The line-emissivity law was defined as $J(r)$ in the thin-disk model by previous authors [8]. It satisfies that $I_e(r, v)=\delta(v - v_e) J(r)$, where $I_e(r, v)$ is the emitted intensity, and v_e is the rest frequency of the emission. Clearly, $J(r)$ is dependent only of r. Note that another expression of J was obtained [31] where J is a function of r, v and θ.

More importantly, the Liouville's equation contains not only the invariant four-momentum of photons, but also the four-velocity & four-coordinate components of particles. The intensity thus depends on more parameters. Let I (ergs s^{-1} cm^{-2} sr^{-1} eV^{-1}) be the specific intensity and N (cm^{-3} dyn^{-3} s^{-3}) the photon distribution function. The relationship between I and N is [26]: $I = 1/2 \times 2hN\nu_e^3$, where h is the Planck constant, v_e =6.35 keV/h is the Kα frequency of a Fe atom with 4-coordinate x^γ and 4-velocity u^γ. Coefficient ½ means that only half of the photons are emitted outwards toward the observer, and 2 indicates that there exist two quantum states per phase-space. The expression of N is written as follows [28]:

$$N\left(x^\gamma, u^\gamma, s^\gamma\right) = C\left(x^\gamma\right) \cdot \delta\left(u^\gamma s_\gamma - h\nu_e\right) \tag{7}$$

where u^γ and s_γ are given in Eq. (3) and (6), respectively. $C(x^\gamma)$ (cm^{-3}) is photon's number density with C=1 according to the previous assumption.

Now let us define two new functions, J_{non-v} and f_v. The former contains all parameters independent of v and the latter contains v-terms only. If it were possible to express the term of $u^\gamma s_\gamma$ in Eq. (7) as a product of $J_{non-v}^{-1} f_v$, the intensity I would then follow $I \propto \delta\left(u^\gamma s_\gamma - h\nu_e\right)\nu_e^3 \propto J_{non-v}\delta(f_v)$, in which J_{non-v} would be a function in the nature of "line-emissivity". Nevertheless, in dealing with the Fe line emission, we do not need to give the analytical expressions of both J_{non-v} and f_v. This is because that (1) numerical computations are irrelevant of analytical expressions; (2) the physics of the line emission is not the same as that of the power-law continuum versus v as assumed in the disk model [5,9]; (3) it is impossible to express the two functions analytically due to the complicated relations among parameters in Eq. (3) and (6).

Flux of line emission

From the line flux, F_{line}:

$$F_{line} = \sum_q \int dv d\Omega \cdot I \cdot \left(\frac{v}{v_e}\right)^3$$

we obtain the expression of the dimensionless flux F as follows:

$$F = \frac{r_0^2}{h\nu_e} F_{line} = \frac{v / v_e}{2E \cdot T_{13} \sin^2\theta_0} \sum_q \int \left\{ \frac{\cos\theta dW^2}{T_{19}\sqrt{W^2 - \left[T_{17} + a(1-\mu)\right]^2}} + \frac{\cos\theta dW^2}{T_{20}\sqrt{W^2 - \left[T_{18} + a(1-\mu)\right]^2}} \right\} \tag{8}$$

in which v/v_e is the general relativistic frequency shift factor. Clearly, F depends on the three parameters: BH spin a, radial position r of the torus emitters, and the inclination angle θ_0 of the observer. The integration over the element of the solid angle $d\Omega$ covers the image of the spherical ring in the observer's sky, while the solid angle is expressed by the impact parameters α and β which are related to the constants of motion [Formula A15, A16 in 9, and Formula (2.3)~(2.5) in 18]. Note that $E = hv$, and $(v/v_e)^3$ arises from along the entire trajectory of the photon. The invariant, $I_v / v^3 = I_{ve} / v_e^3$, is used, which is the result of the conservation of photons in a flux tube, together with the conservation of volume in phase space. The sum Σ is performed to all the values of q to give the total flux contributed by all the photons from all the particles. The intermediate

parameters in Eq. (8) are given as follows:

$$T_{20} = 1 - \frac{(T_{14} - 1) \cdot T_{18}}{\sqrt{T_{15}^2 - T_{16} - (T_{14} - 1) \cdot T_{18}^2}}$$

$$T_{19} = 1 - \frac{(T_{14} - 1) \cdot T_{17}}{\sqrt{T_{15}^2 - T_{16} - (T_{14} - 1) \cdot T_{17}^2}}$$

$$T_{18} = -\frac{T_{15} + \sqrt{T_{15}^2 - T_{14} T_{16}}}{T_{14}}$$

$$T_{17} = -\frac{T_{15} - \sqrt{T_{15}^2 - T_{14} T_{16}}}{T_{14}}$$

$$T_{16} = T_{15}^2 - (1 - \mu) T_{10} (T_{14} - 1)$$

$$T_{15} = -\frac{T_{11} + \frac{E_e}{E^2}}{T_{13}} + a(1 - \mu)$$

$$T_{14} = 1 + \frac{1}{1 - \mu} \left(\frac{T_{12}}{T_{13}} \right)^2$$

$$T_{13} = u^{\varphi}$$

$$T_{12} = u^{\theta}$$

$$T_{11} = u^{t}$$

$$T_{10} = \sqrt{W} \,/\, \sin\theta_0$$

$$T_9 = q$$

$$T_8 = p$$

$$T_7 = \Lambda$$

$$T_6 = \Sigma$$

$$T_5 = \Delta$$

$$T_4 = \coth\theta_0$$

$$\alpha = -s_{\varphi} \csc\theta_0$$

$$\beta = \sqrt{s_{\theta}^2 + a^2 (1 - \sin\theta_0) - s_{\varphi}^2 T_4^2}$$

Our purpose is to predict the three parameters $\{a,r,\theta_0\}$ from the ASCA-observed line emissions by means of numerical data-fit simulations within a full range of $\{a, r, \theta_0\}$={0∼0.999, 0∼99, 0°∼90°} in steps of {0.1°,1,5°}. We consider a same continuum background of a simple power-law plus Galactic absorption, and convolve all the numerical data with the instrument response. However, calculations exhibit little effects of the background. The numerical energy interval is set as 100 keV, approximately the same as the average energy bin-width in the band of 4-7 keV in FIG. 1 of Nandra et al. [6]. The case of a=1 is excluded because any BHs are unable to rotate with such extreme momentum [29]. With the increment of every numerical step, the profile of F changes continuously and it is easy to pick out the best data-fit ones to the ASCA spectra. In view of the data, we hereafter use the nomenclature *Obs* to replace θ_0 in the text.

Sensitivity of torus model

FIG. 2 presents the sensitivity of the torus model. With nine different sets of the three parameters, simulated Fe Kα -line flux F versus the emission energy E (keV) are divided into three groups: (1) the three panels, (b), (e), (h), in the middle column show {a=0.9, 0.95, 0.99}, respectively, at r=25 and *Obs*=50°; (2) the three panels, (d), (e), (f), in the middle row correspond to {r=24, 25, 26 }, respectively, at a=0.95 and *Obs*=50°; (3) the five panels, (e), (a), (c), (g), (i), give the cases that *Obs* is changing from 40° to 60°, respectively, at a=0.95 and r=25.

Although the numerical step of *a* is set as 0.01 from 0.9 to 0.99, three panels in the middle column do not show serious changes in shape. The energy band is slightly widening and the skewed, double-hump profile varies a little with the increase of *a*. However, the flux is obviously influenced by *r* in view of the flux differences in the three panels of the middle row. Although the energy band is nearly constant from 5 keV to 7.5 keV, the profile is nearly a single-peak one at *r*=24. When *r* increases, another hump in the redshift band occurs and at *r*=26, the hump transforms to another peak. The effect of the inclination angle on the flux is the most striking one. In the range of 40°∼60°, the lower hump below 6 keV changes in intensity and merges into the neighbour higher hump.

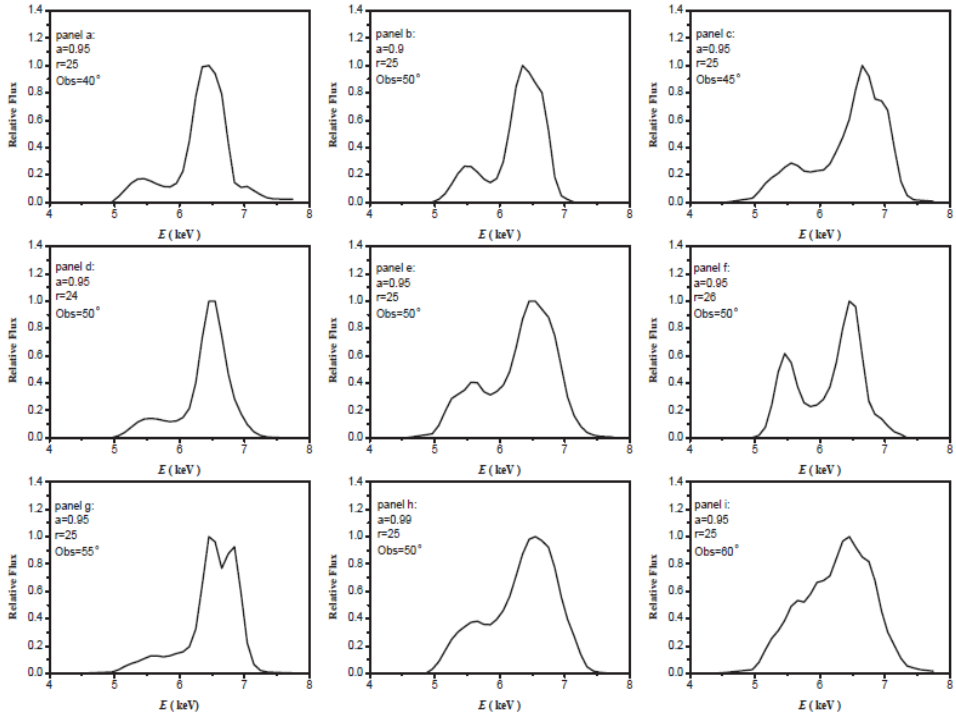

FIG. 2. **Sensitivity of the torus model. The three panels, (b), (e), (h), in the middle column show the flux *F* versus *E* (keV) with {*a*=0.9, 0.95, 0.99}, respectively, at *r*=25, *Obs*=50°; the three panels, (d), (e), (f), in the middle row correspond to {*r*=24, 25, 26}, respectively, at *a*=0.95 and *Obs*=50°; the five panels, (a), (c), (e), (g), (i), give the cases that *Obs* is changing from 40° to 60°, respectively, at *a*=0.95 and *r*=25.**

Flux profile and its dependence on *a*, *r*, and *Obs*

We examine the dependence of the flux profiles under different sets of the three parameters, in order to find the best data, fit curves to the ASCA spectra.

Case 1: Profile as a function of BH's spin *a*:

FIG. 3 and FIG. 4 present partial results at *r*=4, θ_0=30° and *r*=25, θ_0=50°, respectively. At the smaller radius *r*=4, FIG. 3 shows three obvious features: (1) below *a*=0.56, there is no flux; (2) for *a*<0.65 there is only one main peak below∼5 keV while for *a*>0.65, the spectrum occupies the whole band but with a more-extended, higher-humped blue-wing relative to the central emission energy 6.35 keV; (3) the spectral line of a>0.7 is not sensitive to *a*.

On the other hand, at a larger radial position r=25, both nine panels of FIG. 4 and the three middle-column panels of FIG. 2 show following changes: (1) below a=0.006, there is no flux; (2) for a<0.15 there is only one main peak at E>6 keV while for a>0.15 the spectrum occupies the 5–8 keV band with a more-extended red-wing and a higher-humped blue-one; (3) for a>0.6, profiles are similar in shape with the ratio of two peaks less than 4. In general, for any set of {r, *Obs*}, there exists a prescribed minimum of a below which there is no data calculated. This is identical with Wilkins (1972)'s result: For a specific r, stable spherical particles can only exist beyond the minimal spin, a_{min}. This means, below a=0.56 at r=4 or a=0.006 at r=25, there are no stable torus particles around the central BH.

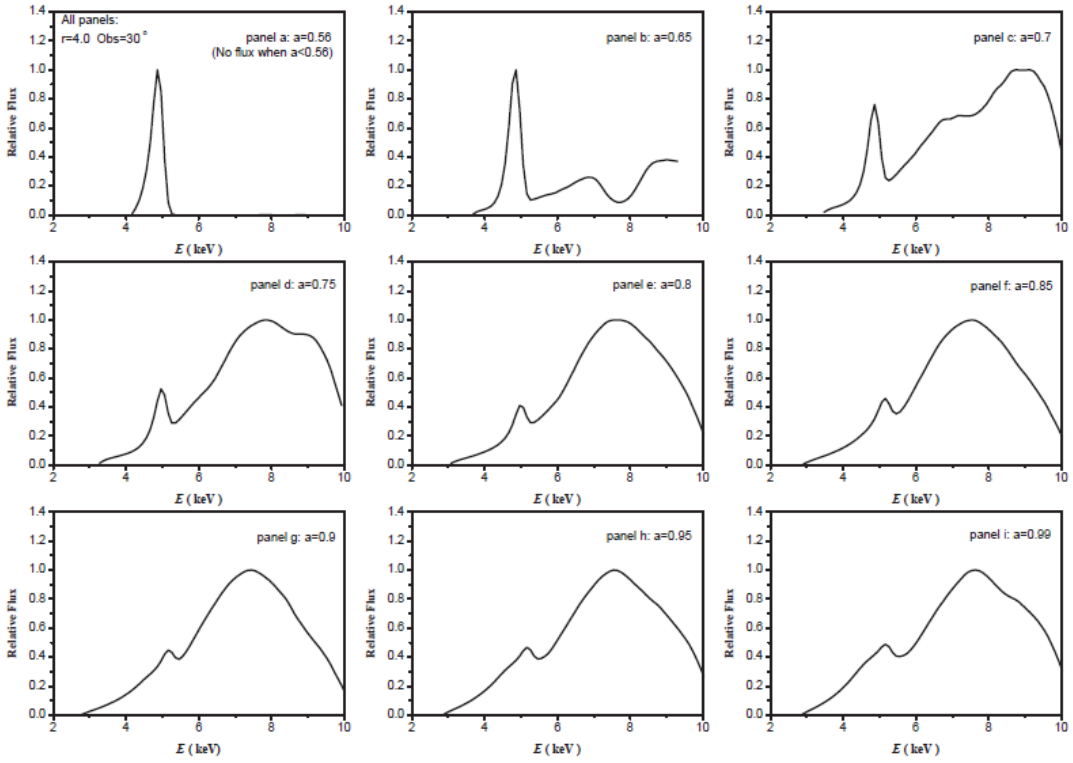

FIG. 3. ***F* as a function of *E* (keV) in cases of different *a* values from (a) to (i) at *r*=4 and *Obs*=30°.**

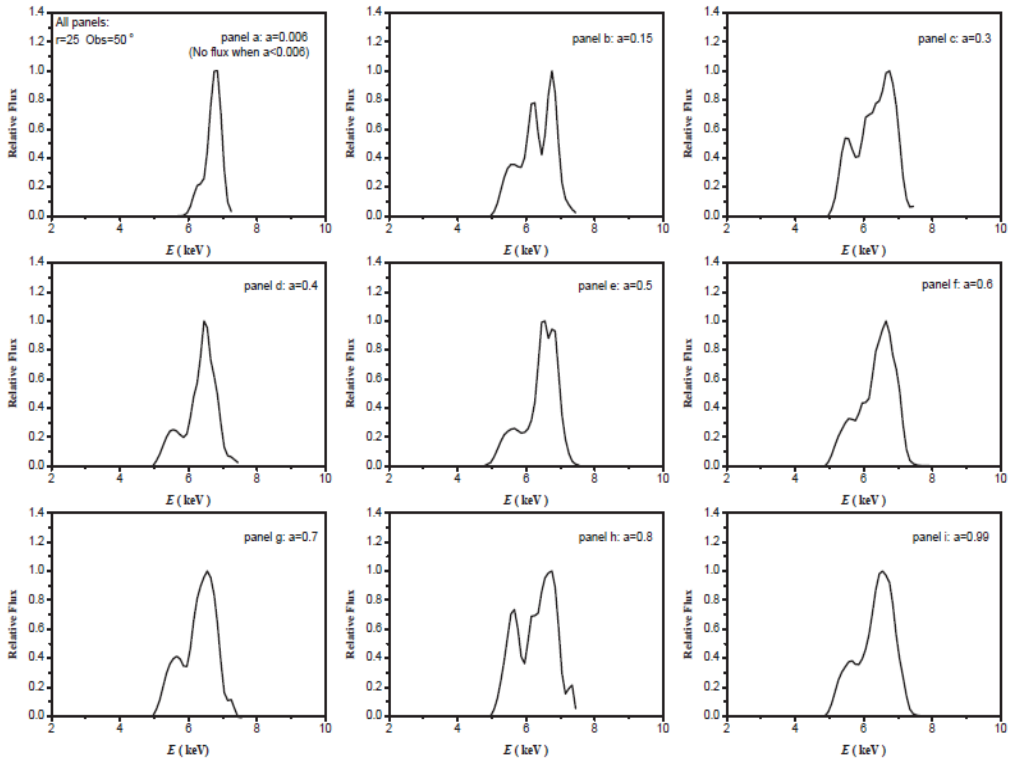

FIG. 4. ***F* as a function of *E* (keV) in cases of different *a* values from (a) to (i) at *r*=25 and *Obs*=50°.**

The result reveals that if any flux is detected, the BH spin a is certainly no less than a_{min}. Calculations verify that in any case no data are produced with the static Schwarzschild case of a=0. This result offers the evidence that the Fe lines convey a clear message about the spinning state of the central body: it is a rotating BH rather than a nonrotating one. Because the simulation is the result of the convolution with ASCA response, it is convincing that the ASCA data provided a definite information to expose that Seyfert AGNs have spinning central cores.

Case 2: Profile as a function of radial position *r*:

FIG. 5 and FIG. 6 give some results of the flux as a function of the radial position r. The former gives nine panels for a smaller inclination angle *Obs*=30° at a=0.99, while the latter, along with the three middle-row panels of FIG. 2, show 12 panels for a larger angle *Obs*=50° at a=0.95.

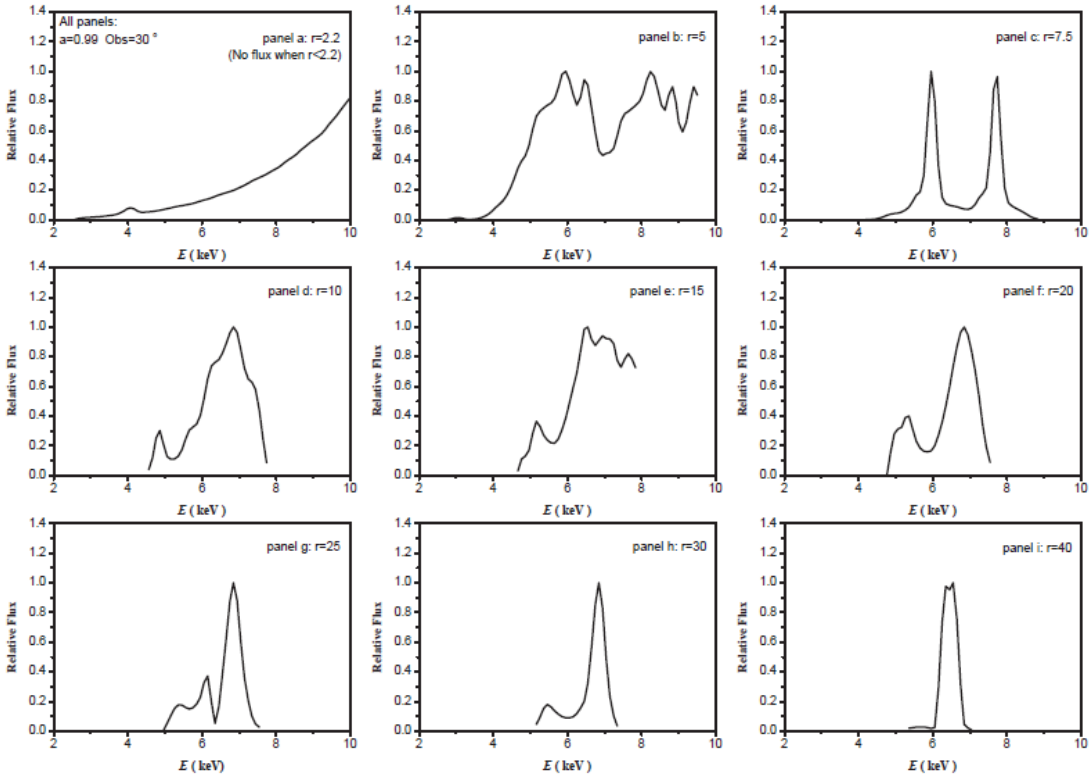

FIG. 5. ***F* as a function of *E* (keV) in cases of different *r* values from (a) to (i) at *a*=0.99 and *Obs*=30°.**

Panels in the two figures suggest that the predicted flux versus the emission energy depends upon the radial position r with following features:

- There exist the minima of r, r_{min}, below which no data is calculated. r_{min}=2.2 in FIG. 5 and r_{min}=2 in FIG. 6. This is in accordance with Wilkins [10]'s work that for a definite value of a, stable spherical particles can only exist outside r_{min}.
- With the increase of r, the profile gradually shrinks into a δ-function. This is what we assumed for the original Fe emission function in the rest frame. Because the closer the test particle to the central body, the stronger the frame-dragging effect of the BH on the particle [10], it is understandable that if the distance to the central BH is sufficiently large, the gravitation cannot exert an effective impact on the frequency-shift and no such information is able to be transmitted outward. Simulations show that for r>40, the emission lines reduce to the conventional δ-function profiles in the absolute space; that is to say, any double-peaked profiles measured by satellites imply that the emissions are from the particles which exist close to the central BHs.
- The region of r=10~40 appears to be the most favourable position for the line emissions. This result is in good agreement with that declared by previous authors [4]. It specifies that the radial position of the illuminating particles cannot be bounded beyond tens of r_g for the emissions of the observed double-humped, broad Fe line spectra.

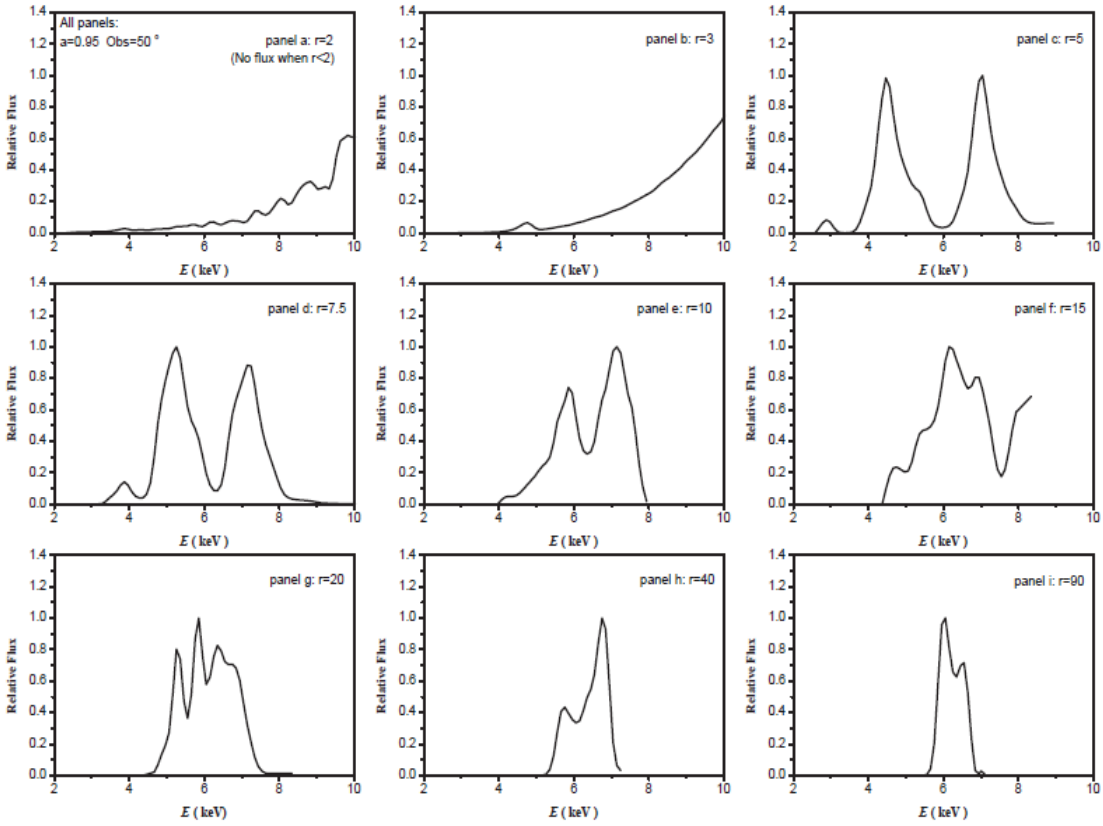

FIG. 6. ***F* as a function of *E* (keV) in cases of different *r* values from (a) to (i) at *a*=0.95 and *Obs*=50°.**

Case 3: Profile as a function of the observer's inclination angle *Obs*:

FIG. 7 and FIG. 8 (accompanied by both the central panel and the four corner ones in FIG. 2) present two examples of the flux versus *Obs* at r=5 and r=25, respectively. Either for a smaller r or a larger r, they show following similar features:

- Except of *Obs*=0° at which the line of sight is along BH's spinning axis, there always exist broad line emissions in the entire scope of 0°<*Obs* ≤ 90°. However, with the increase of the angle, the energy band of all the fluxes does not show appreciable changes.
- After *Obs*>60° at the smaller radius and *Obs*>70° at the larger one, the profiles develop reluctantly. We name this angle, Obs_{const}. after examining all the calculated data, Obs_{const} cannot be smaller than 55° at any r with a=0.99. This feature can help us to judge qualitatively the inclination angle of a BH system.
- Only in the range of *Obs*<70°, can simulations give the spectra which are featured by the usually detected double-humped, broad line profiles. This result supports that obtained from the disk models used for a few Seyfert AGNs [32,33].

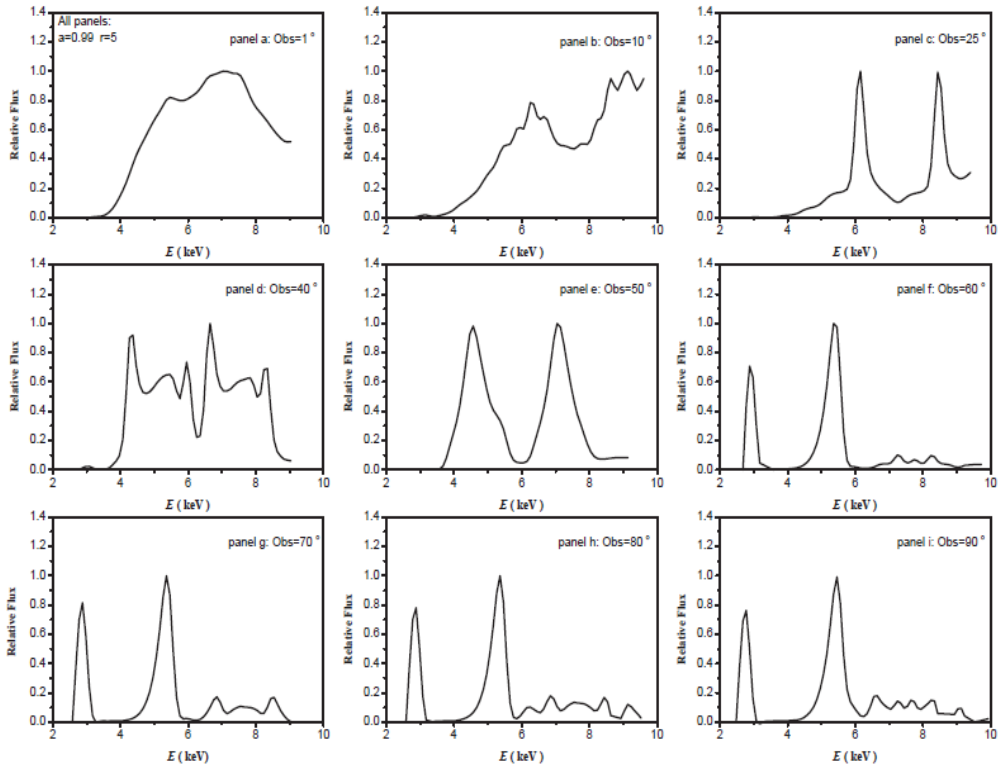

FIG. 7. ***F*** **as a function of** ***E*** **(keV) in cases of different** ***Obs*** **values from (a) to (i) with** ***a*****=0.99 and** ***r*****=5.**

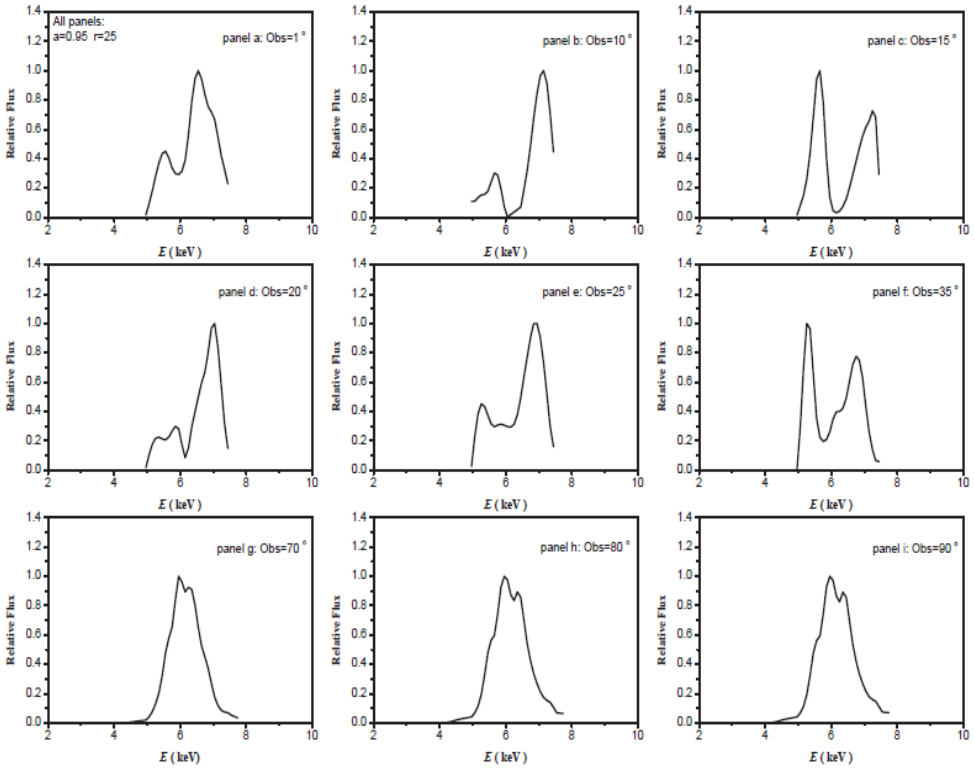

FIG. 8. ***F*** **as a function of** ***E*** **(keV) in cases of different** ***Obs*** **values from (a) to (i) with** ***a*****=0.95 and** ***r*****=25.**

Data-Fit Modelling to NGC 3516 and Discussion

FIG. 9 presents the data-fit to the observation of the Fe Kα emission from NGC 3516 [6]. The band of 4 keV to 7 keV is labelled by two vertical solid lines, where the original data with error-bars are symbolized by black rectangles. The measurement exhibits following features: (1) In the band of 5 keV to 7 keV, there occur two humps, one is located at the lower energy side of 5 keV to 6 keV, and the other at the higher side of 6 keV to 7 keV; (2) Around 5 keV and 6 keV, the profile shows relatively abrupt increases, while in the band of 6.5 keV to 7 keV there is a relatively rapid decrease; (3) At~5.7 keV there occurs a so-called "absorption" which is interpreted as the resonance scattering by iron. Based on these criteria, we made it certain that a simulation profile of {a=0.9, r=25, Obs=50°} can give the best fit to the above observed profile, as shown in the Figure with a pink curve; in addition, we found the profiles within following restrictions also show relatively good fits: {a >0.4, 20< r<40, Obs<50°}. Outside this scope, no favorable fits were presented. Thus, it may be sure that the central BH of NGC 3516 is a rotating object with a>0.4, and, most likely a=0.9. Besides, the radial position of the emitting torus may fall within from $20r_g$ to $40r_g$. Furthermore, the inclination angle of the BH axis may not be larger than 50°.

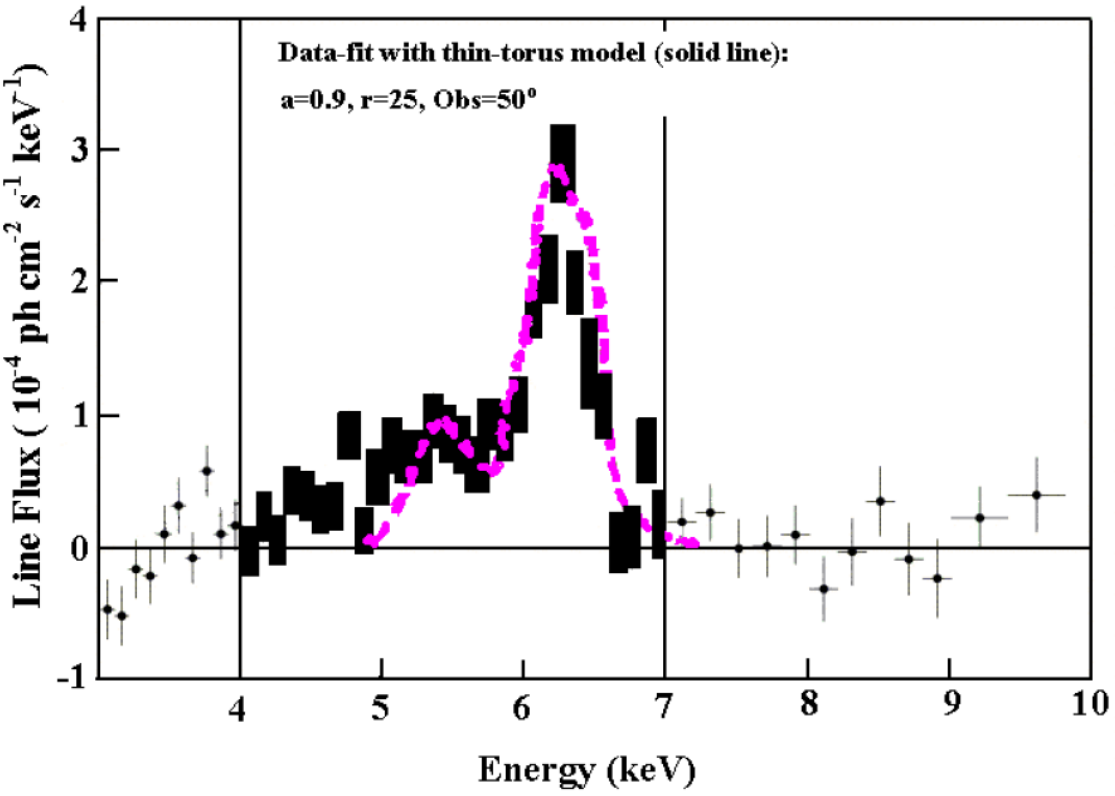

FIG. 9. **Data-fit to the detected data of iron Kα emission in NGC 3516 [6]. The band of 4 keV to 7 keV is labelled by two vertical solid lines in which original data with error-bars are symbolized by black rectangles. The pink curve indicates the best-fit profile with {*a*=0.9, *r*=25, *Obs*=50°}.**

Last but not least, the maximal torus extension to both sides of the equatorial plane is 67.3°. This means that the line emission originates from a torus which extends from −67.3° to 67.3° relative to the equatorial plane. Either from the above data-fits to NGC 3516, or the simulation profiles shown in the last Section, we see that the torus model can provide following two dominant characteristics of the observed Fe line spectra: (1) Humps in both sides of around 6.35 keV, respectively, with an asymmetry to

the red. The red-shifted hump forms a broader wing with a lower peak, while the blue-shifted one, closer to the line emission energy E_e=6.35 keV, gives a relatively narrow but higher component. (2) The so-called "absorption" feature around 6.0 keV. This feature was detected from not only NGC 3516, but also many other Seyfert(-like) galaxies [3,7,34,35]. Nevertheless, we point out, based on our simulations, that the so-called "absorption" may not be real: it seems to be nothing else but only a natural physical expression of the sum of all the individual fluxes with a fovea at that energy. This is because that in the torus formulation of the non-disk particles, we did not consider any other factors, such as, a kind of occultation mechanism or the resonance scattering by iron. Let's discuss a little more about the frequency shifts featured by the spectral troughs and peaks. As discussed in previous studies [4,6,20,35], the shifts are brought about by three shifting-broadening factors: (1) gravitational or general relativistic shift α_1; (2) transverse or special relativistic Doppler shift α_2; and (3) classical or longitudinal Doppler shift α_3.

Because $\alpha_1 = \sqrt{\Sigma\Delta / \Lambda}$ leads only to the redshift of the emission, we concentrate on α_2 and α_3 which contribute to both blue and red shifts. There are altogether two types of particles in the torus: prograde ones (p>0) and retrograde ones (p<0) [see Eq.(5)]. Relative to the observer, each kind of particles is divided further into two halves: the approaching ones and receding ones. Based on previous discussions [5,36], we argue that the four types of particles contribute to the whole profile with humps and troughs: Prograde & approaching particles may bring about the most flux to the blue-shifted hump(s), while retrograde & receding ones to the red-shifted hump(s). If the description is true, the more extended red wing below 6 keV should be caused by a jointly effect of both the retrograde & receding particles and the α_1 factor. More detailed calculations and analyses will be presented in a following paper. We also report another unexpected feature: the blue wing may not be necessarily located in the blue-shifted region of the broad emission line spectra. Our simulations include such results that the blue wing resides actually at the redshift band, while the red wing extends further to the lower energy end in the redshift region. In this case, there is no hump at the energy higher than the rest one of 6.35 keV. That is to say, the synthetic effect of the three shifting-broadening factors drives the whole spectra into the redshift band.

Summary and Conclusion

Since the line emission is a more useful tool than the continuum [20], many studies simulated the line spectra in the regime of the thin-disk model, either for a system hosting a static Schwarzschild BH or a Kerr one. However, there exists the uncertainty about the rotating status of the BH in fitting the disk model to the observed data [6]. Because the thin-disk assumption breaks up in the inner disk surrounding the central BH, we extended the thin-disk model to the thin-torus model in this special region so as to interpret exactly what the observed line spectra tell us. Predicted Fe lines demonstrate that the BH is not a Schwarzschild one but a rotating body. As an attempt, we apply the new model to one sample galaxy, NGC 3516, with the same method used in [20] for MCG-6-30-15. The prior 2002 Letter [23] presented an initial report that NGC 3516 has a central BH of spin a~*0.95*, along with the radial position of an emitting torus r~14 and the observer's inclination angle θ_0~30°. In this paper, we extend the previous work by a detailed formulation of the Fe line emission mechanism and a revisit to the spectra of NGC 3516. More extensive simulations expose following updated results: a is larger than 0.4, with the best-fit value of 0.9. In addition, r is within (20-40) r_g; and, θ_0 of the observer is no larger than 50°. We predict that the torus can extend to both sides of the equatorial plane with a maximal angle of 67.3°. Interestingly, our simulations do not support the so-called "absorption" feature in the Fe line spectra around the energy of 6.0 keV.

It deserves to mention that our torus model is a physical model. It has following assumptions which may deviate from reality:

- In our model, we only considered a thin-torus structure where homogeneous photons are emitted by homogeneous, luminous particles. But real torus around a BH may have a certain thickness (however may be very small) and the line emission, as well as the particle distribution, may not be homogeneous.
- We only dealt with the simplest monochromatic emission. But it is possible that the emission includes other components like Fe Kβ, and/or Ni Kα [6,32].
- In addition to the stable spherical particles, there also exist radially oscillating particles [16,22,25] which may affect the line emissions.

Albeit the fact, the data-fit modelling results in simulating NGC 3516 encourage us to develop this torus model as a useful tool in the diagnoses of the Fe line emissions from more Seyfert(-like) AGNs, while keeping in mind in future studies to check and guarantee the mentioned uncertainties as sufficiently small before simulations, thus, they are unlikely brought into play in the modelling.

REFERENCES

1. Fabian AC, Nandra K, Reynolds CS, et al. On broad iron Hα lines in Seyfert 1 galaxies. MNRAS. 1995;277:L11.
2. Mushotzky RF, Fabian AC, Iwasawa K, et al. Detection of broad iron K lines in active galaxies. MNRAS. 1995;272:L9.
3. Yaqoob T, Serlemitsos P. A Broad Fe Kα Emission Line in the X-Ray Spectrum of the Quasar 3C 273. Astrophys J Lett. 2000;544(2):L95-9.
4. Tanaka Y, Nandra K, Fabian AC, et al. Gravitationally redshifted emission implying an accretion disk and massive black hole in the active galaxy MCG-6-30-15. Nature. 1995;375:659-61.
5. Dabrowski Y, Fabian AC, Iwasawa K, et al. The profile and equivalent width of the X-ray iron emission line from a disc around a Kerr black hole. MNRAS. 1997;288(1):L11-5.
6. Nandra K, George IM, Mushotzky RF, et al. The Properties of the Relativistic Iron K-Line in NGC 3516. Astrophy J Lett. 1999;523:L17.
7. Fabian AC, Rees MJ, Stella L, et al. X-ray fluorescence from the inner disc in Cygnus X-1. MNRAS. 1989;238:729F.
8. Laor A. Line profiles from a disk around a rotating black hole. Lecture Notes in Physics. 2005;385:205-8.
9. Cunningham CT. The effects of redshifts and focusing on the spectrum of an accretion disk around a Kerr black hole. Astrophys J. 1975;202:788-802.
10. Wilkins DC. Bound geodesics in the kerr metric. Phys Rev. D. 1972;5:814-22.
11. Chen K, Halpern JP. Structure of line-emitting accretion disks in active galactic nuclei-ARP 102B. Astrophys J. 1989;344:115-24.
12. Page DN, Thorne KS. Disk-Accretion onto a Black Hole. Time-Averaged Structure of Accretion Disk. Astrophys J. 1974;191:499-506.
13. Collin-Souffrin S, Dumont AM. Line and continuum emission from the outer regions of accretion discs in active galactic nuclei. II. Radial structure of the disc. Astron Astrophys. 1990;229:292-301.
14. Carter B. Global Structure of the Kerr Family of Gravitational Fields. Phys Rev. 1968;174:1559.
15. Bardeen JM, Press W, Teukolsky S. Rotating Black Holes: Locally Nonrotating Frames, Energy Extraction, and Scalar Synchrotron Radiation. Astrophys J. 1972;178:347-70.
16. Stewart J, Walker M. Springer Tracts in Modern Physics. Springer. 1973;69:78.
17. Fang LZ, Zhang JL. Optical appearance of accretion disc around a compact star-Kerr metric. Kexue Tongbao. 1975;20:465.

18. Karas V, Vokrouhlicky D, Polnarev AG. In the vicinity of a rotating black hole - A fast numerical code for computing observational effects. MNRAS. 1992;259(3):569-75.
19. Zakharov AF. On the hotspot near a Kerr black hole: Monte-Carlo simulations. MNRAS. 1994;269(2):283-8.
20. Bromley BC, Chen K, Miller WA. Line Emission from an Accretion Disk around a Rotating Black Hole: Toward a Measurement of Frame Dragging. Astrophys J Lett. 1997;475(1):57-64.
21. Hollywood JM, Melia F. General Relativistic Effects on the Infrared Spectrum of Thin Accretion Disks in Active Galactic Nuclei: Application to Sagittarius A. Astrophys J Suppl Ser. 1997;112(2):423-55.
22. Ma ZG. Geodesics of Bounded Particles around a Kerr Black Hole. Ch A&A. 2000;24:135-44.
23. Ma ZG. Iron Kα Emission Lines in Seyfert (-Like) Active Galactic Nuclei: Revelation of a Rapidly Spinning Central Black Hole. Chin Phys Lett. 2002;19:1537.
24. Ma ZG. High Energy Processes and Phenomena in Astrophysics. In: Li XD, Trimble V, and Wang ZR, editors. IAU. 214:2003;275.
25. Chandrasekhar S. The mathematical theory of black holes. General Relativity and Gravitation. New York: Springer, USA; 1983. p. 5-26.
26. Cameron AGW, Thorne KS. High Energy Astrophysics. In: Dewitt C, Schatzman E, Veron P, editors. New York: Gordon and Breach Science Publishers, USA; 1967. 449p.
27. Ames WL, Thorne KS. The Optical Appearance of a Star which is Collapsing through its Gravitational Radius. Astrophys J. 1968;151:659-70.
28. Gerlach UH. Optical Appearance of a Collisionless Gas of Stars Surrounding a Black Hole. Astrophys J. 1971;168:481.
29. Thorne KS. Disk Accretion onto a Black Hole. II. Evolution of the Hole. Astrophys J. 1974;191:507-19.
30. Iwasawa K, Fabian AC, Reynolds CS, et al. The variable iron K emission line in MCG-6-30-15. MNRAS. 1996;282(3):1038-48.
31. George IM, Fabian AC. X-ray reflection from cold matter in active galactic nuclei and X-ray binaries. MNRAS. 1991;249:352.
32. Wang JX, Zhou YY, Wang TG. The Broad Fe K-Line Profile in NGC 4151. Astrophys J Lett. 1999;523:L129-32.
33. Yaqoob T, George IM, Nandra K, et al. Physical Diagnostics from a Narrow Fe Kα Emission Line Detected by Chandra in the Seyfert 1 Galaxy NGC5548. Astrophy J. 2001;546:759.
34. Stella L. Measuring black hole mass through variable line profiles from accretion disks. Nature. 1990;344:747-9.
35. Weaver KA, Yaqoob T. On the Evidence for Extreme Gravity Effects in MCG-6-30-15. Astrophy J. 1998;502:L139.
36. Lu Y, Yu Q. The Effects of Relativistic Bulk Motion of X-Ray Flares in the Corona on the Iron Kα Line in Seyfert 1 Galaxies. Astrophy J. 2001;561(2):660-75.